

## VALIDATION OF STORAGE MODELS INCLUDED IN THE DIONISIO NUCLEAR FUEL PERFORMANCE CODE: THERMAL MODELS

Francisco Rotea<sup>a,b</sup>, Ezequiel Goldberg<sup>b</sup>, Mauricio E. Cazado<sup>b</sup> and Alejandro Soba<sup>b,c</sup>

<sup>a</sup>*Comisión Nacional de Energía Atómica, Instituto Sabato, Av. Gral. Paz 1499, San Martín, Buenos Aires, Argentina, <https://www.isabato.edu.ar/>*

<sup>b</sup>*Comisión Nacional de Energía Atómica, Gerencia de Área Ciclo del Combustible Nuclear, Sección Códigos y Modelos, Av. Gral. Paz 1499, San Martín, Buenos Aires, Argentina, <http://www.cnea.gov.ar/>*

<sup>c</sup>*Consejo Nacional de Investigaciones Científicas y Técnicas (CONICET), Godoy Cruz 2290, CABA, Buenos Aires, Argentina, <https://www.conicet.gov.ar/>*

**Keywords:** Pool storage, dry storage, spent nuclear fuels, DIONISIO, simulation, finite elements.

**Abstract.** During the storage stage, spent nuclear fuels undergo different thermomechanical stresses that can compromise their integrity, given the long times involved. Experimental data on these processes is not abundant and, in many cases, only simulation codes are available to predict the evolution of these parameters due to the difficulties of carrying out representative experiments. In this work, we present new models added to the storage module of the DIONISIO fuel code, which allow the code to simulate the behaviour of the fuel in each of the storage stages. Models are presented to describe the decay heat as well as the pool and dry storage stages. All these models require validation, either with data measured in different repositories around the globe or with experiments designed to reproduce the storage conditions. This paper presents a selection of validations to ensure the reliability of the models developed within the module.

## 1 INTRODUCTION

The operational lifespan of a nuclear fuel element is relatively short compared to the extended duration it will spend in storage, initially in pools for the first few years, and subsequently in dry storage for decades. Throughout this post-irradiation period, the fuel is subjected to various thermomechanical and thermochemical stresses that can impact its stability. Although these processes may cause only minor changes in the short term, significant alterations can occur over decades, potentially compromising the integrity of the fuel and the safety of containment facilities (Spykman, 2018; Tarn et al., 1986; Alyokhina, 2018; International Atomic Energy Agency, 2004). Conducting experiments to simulate these long-term conditions is not only prohibitively expensive but often impractical due to the extensive timescales and the numerous random factors involved, which require comprehensive statistical sampling (International Atomic Energy Agency, 2004; Peehs and Fleisch, 1986; Graves et al., 2012). As a result, simulation tools have become a cost-effective and viable option for generating predictive insights. Software capable of modeling the entire post-irradiation behavior of nuclear fuels, considering the multitude of interdependent phenomena over hundreds of years, is invaluable to organizations responsible for the storage, conservation and safety of spent fuel elements (Leenaers et al., 2003; Raynaud and Einziger, 2015).

In this context, the Codes and Models Section of the Nuclear Fuel Cycle Department of Argentina's National Atomic Energy Commission (CNEA) has developed the DIONISIO nuclear fuel performance code, currently in version 3.0. This code simulates the behavior of a nuclear fuel rod under irradiation, during normal reactor operation and LOCA-type accident scenarios. The code is currently being extended to include the storage period, creating a comprehensive virtual tool for analyzing the entire lifecycle of a nuclear fuel rod. This paper describes the thermal models used for both pool and dry storage conditions, along with validations using experimental results.

## 2 MODELS

### 2.1 Decay heat

Once the irradiation process is complete and the fuel is removed from the reactor, the fission products generated during reactor operation decay by various mechanisms over the following years, generating waste heat called *decay heat*. The decay heat depends on the total irradiation time of the fuel and is mainly a consequence of the emission of negative beta particles and gamma photons by the irradiation products. In order to model decay heat, two models taken from Ragheb (2014) and Untermeyer and Weills (1952) are used. Both models include the residual power of the entire irradiation history of the fuel, mainly due to the contribution of fission processes determined by the  $^{235}\text{U}$  chain, and the correction introduced when considering the heat generated by the decay of  $^{239}\text{U}$  and  $^{239}\text{Np}$ , both isotopes generated by the neutron capture of  $^{238}\text{U}$  during the operation period.

Both models assume that a fuel is irradiated during a period between  $t = 0$  and  $t = t_0$ . The time  $\tau$  is any instant after the fuel extraction ( $\tau > t_0$ ). To determine the total decay power at time  $\tau$ , all fissions that occurred in the irradiation period must be considered. Thus, power is integrated over all intervals in the power history. First, the power generated in the time period  $t_i$  and  $t_{i+1}$  is calculated, where  $t_i > 0$  and  $t_0 > t_{i+1}$ . Under these considerations, the following equation can be derived, where  $t$  is the time since fuel extraction, in days:

$$P_{(i,i+1)}(t) = P_{0(i,i+1)} \left\{ 6.48 \times 10^{-3} \left[ (t + t_0 - t_{i+1})^{-0.2} - (t + t_0 - t_i)^{-0.2} \right] + 0.0025 \left[ e^{-42.3529t} - e^{-42.3529(t+t_0)} \right] + 0.0013 \left[ e^{-0.2979t} - e^{-0.2979(t+t_0)} \right] \right\} \quad (1)$$

where  $P_{(i,i+1)}(t)$  is power at time  $t = \tau - t_0$  due to the decay of fission products generated in the period  $t_i$  to  $t_{i+1}$  [MWth] and  $P_{0(i,i+1)}$  is the mean power at which the reactor operated in the period  $t_i$  to  $t_{i+1}$ . The last two terms correspond to the  $^{239}\text{U}$  and  $^{239}\text{Np}$  contributions.

The model by [Untermeyer and Weills \(1952\)](#) also takes into account the rate of negative beta particles and gamma photon emission by the fission products, as well as the contribution of the isotopes  $^{239}\text{U}$  and  $^{239}\text{Np}$ . Thermal power is given by:

$$P_{(i,i+1)}(t) = P_{0(i,i+1)} \left\{ 0.1 \left[ (t + t_0 - t_{i+1} + 10)^{-0.2} - (t + t_0 - t_i + 10)^{-0.2} \right] - 0.87 \left[ (t + t_0 - t_{i+1} + 2 \times 10^7)^{-0.2} - (t + t_0 - t_i + 2 \times 10^7)^{-0.2} \right] \right\} \quad (2)$$

where  $t$ ,  $t_0$ ,  $t_i$  and  $t_{i+1}$  are given in seconds instead of days.

Lastly, the total power  $P(t)$  can be calculated by adding all the considered periods:

$$P(t) = \sum_{i=1}^{n-1} P_{(i,i+1)}(t) \quad (3)$$

The code calculates the decay using both models and takes the maximum between them as a conservative measure. It can be seen that the deviation between both models is negligible up to a period of the order of 1 day.

## 2.2 Pool storage

After fuel is removed from the reactor, the initial decay of radioisotopes takes place mainly underwater, in spent fuel pools located near the reactor vessel. In the transition period between both conditions, the fuel continues under a forced convection regime, which is considered by DIONISIO with a duration that can be set by the user. Then, once the pool storage stage starts, a model of natural convection is applied over a hot object (i.e. the spent fuel rod) immersed in an extensive, quiescent fluid (i.e. water). The combined presence of a fluid density gradient (due to the temperature gradient) and a body force proportional to density (gravity) result in the appearance of buoyancy forces. These forces produce a fluid flow near the surface of the body, generating a boundary layer in which there is a velocity gradient and a temperature gradient ([Bergman, 2011](#)). The boundary layer can be laminar or turbulent. For the laminar case, its parameters are described by the mass, linear momentum, and energy conservation equations. Using dimensionless parameters in these equations makes it possible to arrive at the well-known Grashof ( $Gr$ ), Prandtl ( $Pr$ ), and Nusselt ( $Nu$ ) numbers, facilitating a description of the problem based on fluid properties and existing temperatures. To solve the problem of pool storage, there are numerous correlations for thin vertical cylinders with surface temperature ([Minkowycz and Sparrow, 1974](#); [Cebeci, 1974](#); [Popiel, 2008](#)). The model we selected considers a turbulent regime, a slender cylinder, and heat flow as a boundary condition. [Boetcher \(2014\)](#) shows some of the most widespread models for natural convection in vertical cylinders. The correlations derived by [Fujii et al. \(1970\)](#) were found to be the most suitable for the problem in question. [Fujii et al.](#) conducted experiments in vertical cylinders submerged in various liquids, including water, and established correlations to determine the local Nusselt number for both laminar and

turbulent flows, using uniform heat flow or uniform surface temperature as boundary conditions. In DIONISIO, the problem is solved by calculating the Nusselt number at the midpoint of each axial rod sector and assigning that value to the entire region. Then, the convection heat transfer coefficient is calculated for each sector, followed by the surface temperature ( $T_s$ ) using Newton's cooling law. The Fujii correlations for  $Pr = 5$  and heat flux as initial conditions are expressed in the following equations:

$$\begin{aligned} &\text{for laminar regime, } 10^8 < Gr_x^* Pr < 10^{13} : \\ &(Nu_x)_e = 0.580 (Gr_x^* Pr)_e^{1/4} \end{aligned} \quad (4)$$

$$\begin{aligned} &\text{for turbulent regime, } 10^{13} < Gr_x^* Pr < 10^{15} : \\ &(Nu_x)_e = 0.215 (Gr_x^* Pr)_e^{1/4} \end{aligned} \quad (5)$$

where:

$$Gr_x^* = Gr_x Nu_x = \frac{g \beta q'' x^4}{k \nu^2} \quad (6)$$

where  $g$  is the gravitational acceleration [ $m/s^2$ ],  $\beta$  is the average volumetric thermal expansion coefficient [ $1/^\circ C$ ],  $q''$  is the heat flux at the wall of the heated cylinder [ $W/m^2$ ],  $k$  is the thermal conductivity [ $W/m^\circ C$ ],  $\nu$  is the kinematic viscosity [ $m^2/s$ ] and  $x$  is the distance vertically upward from the lower end of the heated cylinder [ $m$ ]. Equation (6) is known as the modified Grashof number. The subscript  $(\cdot)_e$  indicates that the liquid properties need to be calculated at reference temperature  $T_e$  (Eq. 7), except for the thermal expansion coefficient  $\beta$ , which must be calculated at average temperature  $T_m$  (Eq. 8).

$$T_e = T_s - \frac{1}{4} (T_s + T_\infty) \quad (7)$$

$$T_m = \frac{1}{2} (T_s + T_\infty) \quad (8)$$

where  $T_s$  is the temperature on the heated cylinder wall [ $^\circ C$ ] and  $T_\infty$  is the temperature in the ambient fluid [ $^\circ C$ ]. To implement the correlation, one begins with an arbitrary surface temperature  $T_s$ , calculates  $T_m$  and  $T_e$ , and uses these to evaluate the properties of the water. The correlation is then applied to determine the convection coefficient, which is subsequently used to calculate the new surface temperature  $T_s$ . This iterative process is repeated until convergence is achieved. The water properties used are the ones already included in DIONISIO from the normal operation condition.

### 2.3 Dry storage

Once the pool stage is over, the spent fuels are transferred to dry storage. There are different designs of containers, although, in general, they are metal compartments where the fuel elements are placed in either rectangular or circular arrangements. The fuel elements are usually enclosed in an inert nitrogen (N) atmosphere, with the container surrounded by a layer of concrete that isolates the contents from the outside. Some designs allow airflow between the concrete and the metal, to remove the heat generated inside the container due to radioactive decay.

To model the behavior of a spent fuel rod in dry storage, it is essential to establish the conditions of the rod within a canister. This allows for determining the external temperature

distribution it is subjected to, thereby generating the necessary boundary conditions. To achieve this, a subroutine has been developed that, based on the thermohydraulic conditions of a dry repository and the corresponding atmospheric conditions, calculates the temperature of the rod under the most demanding system conditions. In addition, the user can select other rods under different conditions for more detailed studies, as the model generally reproduces the thermal conditions of all rods within the canister.

The main numerical model on which DIONISIO works is the finite element method. Therefore, for each type of canister to be simulated, the code must be provided with an appropriate mesh that must follow certain parameters required by the model. In this work we have simulated two types: a VSC-17 cask consolidated fuel canister (Lambert, 1992) and the dry repository designed for Atucha (CNA) I and II Nuclear Power Plants (NPPs) in Argentina (Hilal et al., 2017). The reason for this selection was based on the availability of the complete information to generate the mesh. In the future, if a simulation is needed for a different type of canister, a detailed layout will be required to generate the corresponding finite element mesh.

In both cases, we have selected eight different materials in their composition, as can be seen in Figure 1. Three different types of thermohydraulic conditions can be selected by the user, depending on the application zone:

- Convective atmosphere outside the concrete that surrounds the canister.
- Inner air ring, which can be composed of convective air connected to the outside, or sealed air.
- Internal atmosphere with nitrogen (N) or helium (He) filling gas, which in turn can have natural convection or be completely sealed.

Inside each canister, we included each rod with the corresponding Zircaloy cladding and gap between them, filled with an atmosphere of N. In the case of the VSC-17 cask, there is a Multi-Assembly Sealed Basket (MSB) that is filled with He or N, a parameter that can be chosen by the user. In concentric circles, there is the MSB made of steel, the annulus of convective air, the steel liner, and the insulating concrete. Inside the basket, we consider that the filling gas can extract heat through conduction, convection, and radiation. The boundary condition of the model is defined by the ambient temperature surrounding the concrete cask. We also developed a CNAI/CNAII cask model to simulate the repositories designed in Argentina for the fuel elements of both NPPs. The fuel element rods, each 5.6 m long, are arranged in circular

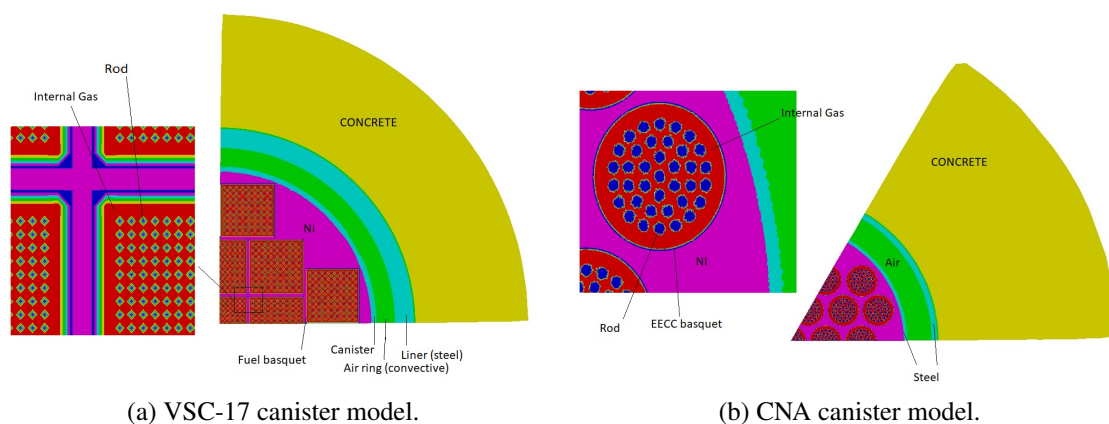


Figure 1: Discretization of the domain using the symmetry of the system.

bundles of 37 rods, which are distributed in concentric circles of 1, 6, 12, and 18 rods per circle. The cask is made of a concrete layer, a steel liner, an airtight ring, and a steel canister that contains 31 fuel elements within steel tubes. All of them are inserted in a N atmosphere. Each rod generated 4.5 W approximately. We consider heat removal by conduction and convection into the air ring and the N. Within the fuel element tubes, we add the radiation mechanism to calculate the effective conduction coefficient.

In Table 1 we summarized the effective conductivity ( $k_{\text{eff}}$ ) model selected for each material in our system.  $\rho_T$  is the thermal resistivity for each rod in the basket [mK/W], calculated using the three materials in series: gap, cladding, and external atmosphere (considering concentric cylinders).

$$\rho_T = \frac{\ln\left(\frac{r_{\text{int.clad}}}{r_{\text{fuel}}}\right)}{k_{\text{gap}}} + \frac{\ln\left(\frac{r_{\text{ext.clad}}}{r_{\text{int.clad}}}\right)}{k_{\text{clad}}} + \frac{\ln\left(\frac{r_{\text{ext.clad}+\Delta r}}{r_{\text{ext.clad}}}\right)}{k_{\text{int.atm.}}} \quad (9)$$

where  $r_{\text{fuel}}$  is the radius of the fuel pellet [m],  $r_{\text{int.clad}}$  and  $r_{\text{ext.clad}}$  are the internal and external radius of the cladding [m] respectively, and  $r_{\text{ext.clad}+\Delta r}$  corresponds to a small distance beyond the external cladding radius [m]. Thermal conductivities of the gap, cladding and internal atmosphere are given by  $k_{\text{gap}}$ ,  $k_{\text{clad}}$  and  $k_{\text{int.atm.}}$  [W/mK].  $h_{\text{rad}}$  is the radiative heat transfer

Table 1: Conductivity model used for each material.

Material	Model	$k_{\text{eff}}$	Ref.
Fuel	Conduction	$k_{\text{UO}_2}$	Soba (2007)
Int. Basket	Serial conduction of gap+cladding+ $\delta_{\text{clad}}$ in parallel with convection+radiation	$\frac{1}{\rho_T} + \frac{1}{F}\Delta_{\text{bas}}h_{\text{rad}} + \Delta_{\text{bas}}h_{\text{conv}}$	Parra and Parkansky (2016)
$\Delta$ Basket-Container	Radiation	$\frac{1}{F}\Delta_{\text{BC}}h_{\text{rad}}$	Incropera and Witt (1999)
Container (steel)	Conduction	$k_{\text{steel}}$	Hagrman (1993)
Canister int. atm.	Serial conduction and radiation	$\frac{1}{F}\Delta_{\text{can}}\frac{k_{\text{gas}}h_{\text{rad}}}{k_{\text{gas}}+\Delta_{\text{gas}}h_{\text{rad}}}$	Incropera and Witt (1999)
Canister (steel)	Conduction	$k_{\text{steel}}$	Hagrman (1993)
Air ring (conv.)	Convection	$\Delta_{\text{air}}h_{\text{convair}}$	Incropera and Witt (1999)
Air ring	Parallel conduction and radiation	$k_{\text{air}} + \frac{1}{F}\Delta_{\text{air}}h_{\text{radair}}$	Parra and Parkansky (2016)
Liner (steel)	Conduction	$k_{\text{steel}}$	Hagrman (1993)
Concrete	Conduction	$k_{\text{concrete}}$	Powell et al. (1966)

$k_i$  : thermal conductivity of material  $i = \text{UO}_2, \text{steel}, \text{concrete}$  [W/mK]

$\Delta_i$  : effective thickness of material  $i = \text{bas}$  (basket),  $\text{can}$  (canister),  $\text{BC}$  (basket-container gap),  $\text{gas}$  (N or He),  $\text{air}$  [m]

$h_{\text{conv}}$  : convective heat transfer coefficient for internal gas [W/m<sup>2</sup>K]

$h_{\text{convair}}, h_{\text{radair}}$  : convective and radiative heat transfer coefficients for air [W/m<sup>2</sup>K]

coefficient [ $\text{W}/\text{m}^2\text{K}$ ], given by:

$$h_{rad} = \sigma_S \frac{(T_{surf}^2 + T_{env}^2)(T_{surf} + T_{env})}{\frac{1}{\varepsilon_{surf}} \left( \frac{1}{\varepsilon_{surf}} - 1 \right)} \quad (10)$$

where  $\sigma_S$  is the Stefan–Boltzmann constant [ $\text{W}/\text{m}^2\text{K}^4$ ],  $T_{surf}$  is the temperature at the rod surface [K],  $T_{env}$  is temperature of the environment far from the surface [K] and  $\varepsilon_{surf}$  is the emissivity of the surface emitting the radiation [1].

The shape factor  $F$  for emission surfaces is 1.0 for rectangular distributions and 0.5 for circular distributions. The convective heat transfer coefficient for air,  $h_{conv,air}$  is  $0.005 \text{ W}/\text{cm}^2\text{K}$ , while for airtight conditions it is  $0.00001 \text{ W}/\text{cm}^2\text{K}$  (Powell et al., 1966; Incropera and Witt, 1999). A similar behavior is observed for  $h_{conv}$  when nitrogen or helium are used as the filling gas. The conductivities, which depend on the material and temperature, were taken from references given in Table 1. The emissivity coefficient,  $\varepsilon_{surf}$ , varies from 0.20 to 0.35, depending on whether the surface material is steel or Zircaloy (Incropera and Witt, 1999).

### 3 VALIDATION

#### 3.1 Experimental test

A performance test was conducted on a Pacific Sierra Nuclear VSC-17 ventilated concrete storage cask configured for pressurized-water reactor (PWR) spent fuel. The test involved loading the VSC-17 cask with 17 canisters of consolidated PWR spent fuel from Virginia Power's Surry and Florida Power & Light's Turkey Point reactors (Lambert, 1992). During the test, temperatures were measured on the cask surface, concrete insulator, air channel surfaces, and fuel canister guide tube. In addition, gamma and neutron dose rates on the cask surface were recorded. The experiment was performed in vacuum, nitrogen, and helium backfill environments, with the cask in a vertical orientation. A total of 98 thermocouples were distributed throughout the basket, including several placed inside the canisters, to measure the temperature of the claddings. Helium and nitrogen were used as backfill gases in the MSB. Temperature measurements were taken at various axial positions within the canister under both gas atmospheres. Data on spent fuel integrity were also collected.

#### 3.2 VSC-17

The VSC-17 system consists of a cylindrical Ventilated Concrete Cask (VCC) and a Multi-Assembly Sealed Basket (MSB) that holds 17 canisters, each containing 408 irradiated PWR rods. The VCC features a reinforced concrete body with an inner steel cylindrical liner. The MSB includes a guide sleeve assembly for fuel support and a composite shield lid that seals the stored fuel. The cavity atmosphere is helium at slightly subatmospheric pressure, which enhances heat transfer and prevents oxidation of the fuel and corrosion of the basket components. There is an annular airflow path of approximately 8 cm in width between the liner and the MSB. Inside the basket, 17 square canisters, each with sides measuring 21.6 cm and a height of 405 cm, are evenly spaced. Each canister has a power output ranging from 700 W to 1050 W, with an average result of approximately 866 W per canister. The dimensions of the cask are 256.54 cm in diameter and 574.0 cm in height.

### 3.3 Results

The model is started by creating a discrete mesh of the domain. Due to symmetry reasons, only  $\frac{1}{4}$  of the domain is modeled. The materials of each portion of the domain must be defined in the DIONISIO library, along with the models for the various thermal constants. The inputs for the model include the power of each rod and the number of rods inside each canister. The power of each rod is calculated in the main program of DIONISIO, based on the fuel's decay function and its irradiation history.

For VSC-17 the mesh has 23233 linear quadrilateral elements. The main code calls the repository subroutine with the power of each rod to calculate the temperature distribution. After that, the subroutine determines the maximum temperature corresponding to the cladding under the most demanding conditions within the domain. Results for the radial and axial temperature distributions are shown in Figure 2.

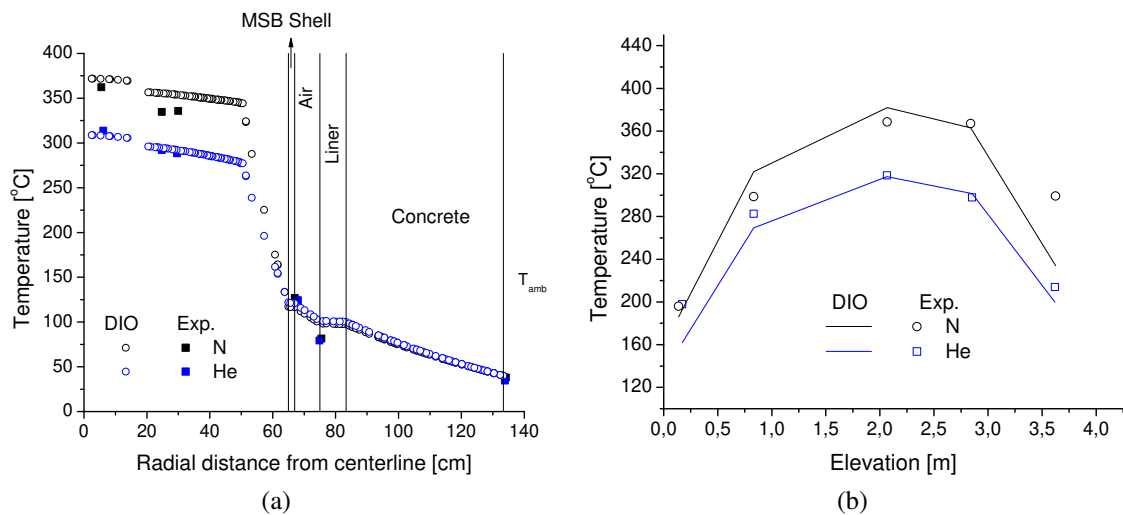


Figure 2: (a) Radial simulated temperature in comparison with experimental values and (b) axial distribution of temperatures in comparison with experimental values.

The results of the performance test indicate that the VSC-17 cask exhibited good heat transfer performance when dissipating 14.9 kW. The maximum measured canister guide tube temperatures in nitrogen and helium backfills in a vertical cask orientation were 366 °C and 316 °C, respectively. Fuel temperatures were less than the 340 °C allowable for the fuel elements when using helium in the cask and with limited blockage of the inlet air vents. Maximum concrete temperatures were about 70 °C for open cooling air vents regardless of backfill.

Figure 3 shows the results of the temperature distribution maps calculated using the model. For the case of the CNA canister, no experimental data is available for comparison. Nevertheless, we estimate the temperature of the most demanding rod to be 375 °C, which is within the expected values for this type of cask.

## 4 CONCLUSIONS

In this work, we present thermal models developed for the new storage module of the DIONISIO nuclear fuel code. Models include decay heat due to the radioactive decay of fission products, natural convection during the pool storage period, and the thermal behavior of dry storage casks. We present validation of canister models compared with experimental results and estimate the value of the most demanding rod in the CNA model, which is always below

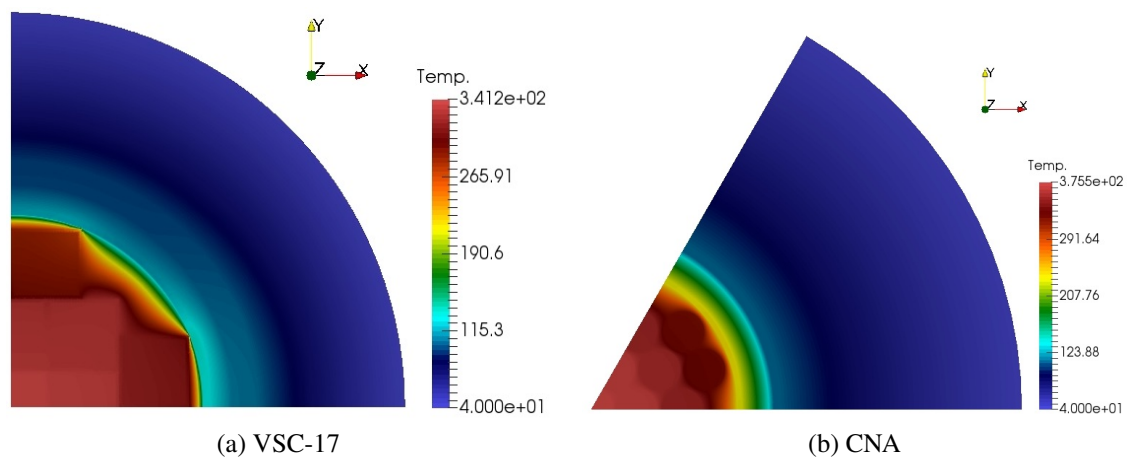


Figure 3: Temperature distribution maps.

400 °C, a limiting condition imposed by the hydrides behavior in Zircaloy claddings (Billone et al., 2013; Woo and Lee, 2023).

Future work involves implementing and validating mechanical and hydrogen behavior models for the storage stage. In terms of mechanical models, creep is known to be the dominant mechanism for cladding deformation under normal storage conditions, due to the relatively high temperatures and hoop stresses on the cladding during this period. For hydrogen behavior, it is understood that during the vacuum drying stage prior to dry storage, temperatures can reach 400 °C with hoop stresses up to 140 MPa (Billone et al., 2013), caused by the increased internal rod pressure from fission gas release and pellet swelling. During cooling, if the hoop stress exceeds a critical threshold, radially oriented hydrides may precipitate. The presence of these hydrides significantly degrades the mechanical properties of the cladding (Woo and Lee, 2023), making it a crucial factor to consider in simulations.

## REFERENCES

- Alyokhina S. Thermal analysis of certain accident conditions of dry spent nuclear fuel storage. *Nuclear Engineering and Technology*, 50, 2018. ISSN 2234358X. doi:10.1016/j.net.2018.03.002.
- Bergman T. *Fundamentals of Heat and Mass Transfer*. John Wiley & Sons, 2011.
- Billone M.C., Burtseva T.A., and Einziger R.E. Ductile-to-brittle transition temperature for high-burnup cladding alloys exposed to simulated drying-storage conditions. *Journal of Nuclear Materials*, 433:431–448, 2013. doi:10.1016/J.JNUCMAT.2012.10.002.
- Boetcher S.K.S. Natural convection from circular cylinders. *SpringerBriefs in Applied Sciences and Technology*, 2014. ISSN 21915318. doi:10.1007/978-3-319-08132-8.
- Cebeci T. Laminar-free-convective-heat transfer from the outer surface of a vertical slender circular cylinder. In *International Heat Transfer Conference 5*, pages 15–19. 1974. doi:10.1615/IHTC5.2830.
- Fujii T., Takeuchi M., Fujii M., Suzuki K., and Uehara H. Experiments on natural-convection heat transfer from the outer surface of a vertical cylinder to liquids. *International Journal of Heat and Mass Transfer*, 13:753–787, 1970. ISSN 0017-9310. doi:10.1016/0017-9310(70)90125-0.
- Graves F.C., Geronimo M.R., and Graves G.A. *Centralized Dry Storage of Nuclear Fuel: Lessons for U.S. Policy from Industry Experience and Fukushima*. 2012.

- Hagrman D.T. *SCDAP/RELAP5/MOD3.1 Code Manual Volume IV: MATPRO. A Library of Materials Properties for Light-Water-Reactor Accident Analysis*. Idaho National Engineering Laboratory, Office of Nuclear Regulatory Research, U. S. Nuclear Regulatory Commission, 1993.
- Hilal R.E., Garcia J.C., and Delmastro D.E. *Cálculo térmico de un sistema para el almacenamiento en seco del combustible gastado CNA1*. CNEA, 2017.
- Incropera F.P. and Witt D.P.D. *Fundamentos de transferencia de calor*. Pearson Educ., 1999.
- International Atomic Energy Agency. *WWER-440 Fuel Rod Experiments Under Simulated Dry Storage Conditions*. number 1385 In TECDOC Series. IAEA, Vienna, 2004.
- Lambert R.W. *TR-100305 Research Project 3073-1 PNL-7839 UC-85, Performance Testing and Analyses of the VSC-17 Ventilated Concrete Cask*. Electric Power Research Institute, 1992.
- Leenaers A., Sannen L., den Berghe S.V., and Verwerft M. Oxidation of spent  $\text{UO}_2$  fuel stored in moist environment. *Journal of Nuclear Materials*, 317, 2003. ISSN 00223115. doi: 10.1016/S0022-3115(03)00104-1.
- Minkowycz W.J. and Sparrow E.M. Local nonsimilar solutions for natural convection on a vertical cylinder. *Journal of Heat Transfer*, 96(2):178–183, 1974. ISSN 0022-1481. doi: 10.1115/1.3450161.
- Parra S. and Parkansky D. *Mecanismos de transferencia de calor. Aire húmedo y mecánica de fluidos*. CNEA, 2016.
- Peehs M. and Fleisch J. LWR spent fuel storage behaviour. *Journal of Nuclear Materials*, 137, 1986. ISSN 00223115. doi:10.1016/0022-3115(86)90219-9.
- Popiel C.O. Free convection heat transfer from vertical slender cylinders: A review. *Heat Transfer Engineering*, 29(6):521–536, 2008. doi:10.1080/01457630801891557.
- Powell R.W., Ho C.Y., and Liley P.E. Thermal conductivity of selected materials. *NSRDS-NBS*, vol. 8 Is. 25, 1966.
- Ragheb M. Decay heat generation in fission reactors. *Lectures*, page Chapter 8, 2014.
- Raynaud P.A. and Einziger R.E. Cladding stress during extended storage of high burnup spent nuclear fuel. *Journal of Nuclear Materials*, 464, 2015. ISSN 00223115. doi:10.1016/j.jnucmat.2015.05.008.
- Soba A. *Simulación del comportamiento termo-mecánico de una barra combustible en operación*. PhD thesis, Universidad de Buenos Aires, Buenos Aires, Argentina, 2007.
- Spykman G. Dry storage of spent nuclear fuel and high active waste in Germany—Current situation and technical aspects on inventories integrity for a prolonged storage time. *Nuclear Engineering and Technology*, 50, 2018. ISSN 2234358X. doi:10.1016/j.net.2018.01.009.
- Tarn J.C.L., Madsen N.H., and Chin B.A. Predictions of dry storage behavior of Zircaloy clad spent fuel rods using deformation and fracture map analyses. 1986.
- Untermyer S. and Weills J.T. Heat generation in irradiated uranium. *U.S. Atomic Energy Commission, Technical Information Service*, 1952. doi:10.2172/4376281.
- Woo D. and Lee Y. Understanding the mechanical integrity of Zircaloy cladding with various radial and circumferential hydride morphologies via image analysis. *Journal of Nuclear Materials*, 584:154560, 2023. doi:10.1016/J.JNUCMAT.2023.154560.